Desalination 460 (2019) 28–40

Contents lists available at ScienceDirect

Desalination

journal homepage: www.elsevier.com/locate/desal

Modeling and simulation of the dual stage pressure retarded osmosis systems

Roghayeh Soltani*, Henning Struchtrup

Department of Mechanical Engineering, University of Victoria, Victoria, BC, Canada

ARTICLE INFO

Keywords:
Pressure retarded osmosis
Dual stage system
Scaled up module
Modeling
Process characteristics

ABSTRACT

Utilization of renewable energy sources, as an approach to reduce Greenhouse Gas (GHG) Emissions, has been globally popular in the last few decades. Among renewable energy sources, pressure retarded Osmosis (PRO) has been scrutinized by scientists since the mid-70's. However, even today, the existing PRO systems can only marginally meet the generally approved criterion of 5 W/m^2 power density, a threshold for an economically feasible river-sea PRO system. As an approach to increase the performance of PRO systems, multi-staging of PRO modules is investigated in this paper.

For this purpose, a number of models for scaled up dual stage PRO power plants with different configurations and target functions are presented and compared to a single stage system with the same membrane area. These models consider the pressure and flow drop as well as the salinity change along the membrane. The results indicate that overall performance of the system could be improved by up to 8% with a dual stage PRO in the case of specific energy. Finally, a thermodynamic analysis addresses the sources for irreversible losses, and the contribution from each source.

1. Introduction

Osmotic energy, besides its other applications such as desalination, food preservation and medicine, is considered as a renewable source of energy [1]. This form of energy is released when two solutions with different salt concentrations are mixed in a membrane module at appropriate pressures. The worldwide capacity of osmotic pressure to generate energy has been estimated to be 2 TW, which is almost 13% of global energy consumption [2]. The solution with a lower salt concentration is called the feed solution, while the higher concentrated solution is referred to as the draw solution. When draw and feed solutions enter the different sides of the membrane module, there is a driving force for fresh water to permeate from the feed (diluted) to the pressurized draw solution (concentrated). The process is continued as long as the difference in the hydraulic pressure is less than the difference in the osmotic pressures.

Pressure is applied to the draw solution side to retard water permeation from the feed solution to the draw solution through the membrane. Constant energy generation is obtained by depressurizing the permeate through the hydroturbine, the method is called Pressure Retarded Osmosis (PRO) [3]. The hydraulic pressure must not exceed the osmotic pressure difference in the system which is the driving force of water permeation. Osmotic pressure is related to the difference in salt concentrations of draw and feed solutions. Therefore, the higher this difference is, the higher the osmotic pressure difference will be. Hence, sources with higher salt concentrations can be considered as draw solutions, such as the Dead Sea [4], brine of desalination plants [5], or ammonia-carbon dioxide [6]. A pilot scale power plant, harvesting PRO energy from sea water was developed in Norway by Statcraft in 2009. However, mainly due to the inefficiency of the membrane causing low generation of power per membrane area (0.5 W/m^2) [7], but also due to low osmotic pressure driving force of chosen draw and feed solution sources [8], this power plant was shut down in 2012.

In order for a PRO power plant to be commercially feasible, it is estimated that the power density should be above 5 W/m^2 [9]. Recently, there have been improvements in membranes and their parameters, especially in laboratory scale power plants [10]. Other factors also affect the power density such as pressure drop along the membrane, operating condition, and PRO configuration. As the scale of the system grows, the mentioned factors play a more vital role and become more important to observe.

In the past few years, PRO was considered as a part of hybrid systems, mostly to recover energy from other osmotic processes such as forward osmosis (FO) or reverse osmosis (RO) [11-13]. The waste of desalination systems, which is concentrated brine, can be used in PRO systems to create some of the power required for desalination [14]. In

* Corresponding author.
E-mail address: ssoltani@uvic.ca (R. Soltani).

https://doi.org/10.1016/j.desal.2019.02.010
Received 25 June 2018; Received in revised form 21 January 2019; Accepted 17 February 2019

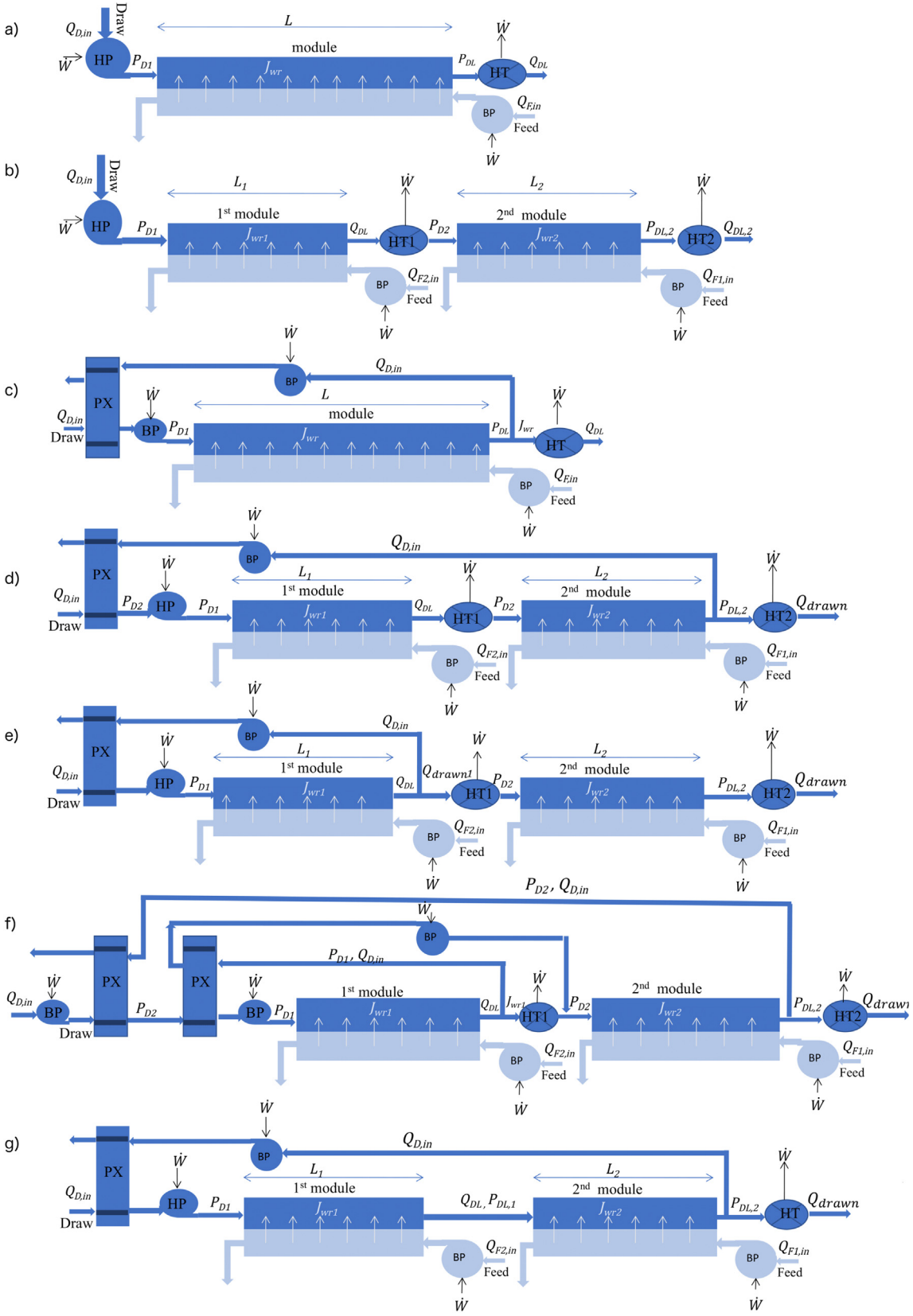

Fig. 1. Schematic of single and dual stages PRO systems with the same membrane area: (a) Single stage with P-T; (b) single stage with PX; (c) dual stage with P-T; (d) dual stage with 1PX; (e) dual stage PRO with Q_D,in back to PX before the HT1; (f) dual stage with 2PX; (g) dual stage system with 1HT.

addition, dual stage PRO configurations have been investigated to improve energy generation. He et al. [15,16] introduced dual stage PRO and studied four configurations, either with continuous or divided flow of draw and/or feed solution. All configurations utilized energy recovery systems and pump-turbine pairs. The hydraulic pressure applied to the draw solution was constant, and the system was optimized to maximize the average power density [16]. Another study for dual stage PRO was conducted by Altaee et al. [17,18] in which two configurations of dual stage PRO are suggested. Both configurations utilize counter-current flow of draw and feed solutions, pressure exchanger (PX) and pump-turbine pair. Similar to [15,16], they have the same applied hydraulic pressure for both modules. Compared to [17], in [18] the system has been modified such that the required volumetric flow of draw solution for PX is extracted at the end of the second module instead of the first. With this change, the input flow for the draw solution in the second module, and subsequently the power density, was increased [18].

In 2016, Straub et al. [19] and O'Toole et al. [20] criticized the viability of power generation from river-sea PRO power plants in terms of net work per inlet flow rates of draw and feed solutions (specific energy, SE), and the net work per drawn fresh water, respectively. They stated that net positive extractible energy is hard to achieve or even impossible. With dual stage PRO, the energy output can be improved to positive numbers [17]. Considering the water quality in British Columbian rivers, the work required for pretreatment of the feed solution, which is considerable (estimated around 0.1 –0.4 $kWhm^{-3}$ [19]), can be ignored or kept at minimum level.

In general, dual stage systems may utilize the advantages of flexibility in selection of membrane types, module configurations, and draw and feed solution sources. Furthermore, low concentrated fresh water entering the second module may cause additional water permeation through the membrane; thereby, increasing power output.

In this paper, large scale dual stage PRO systems in new configurations are presented and compared with a single stage system. In terms of capital cost, dual stage PRO modules may need more membrane area than the single stage PRO and require additional turbo machinery (Pump-Turbine-Pressure Exchanger). In this paper the same membrane area is assumed but some additional turbo machinery is required in the second module. In addition to the other benefits of a dual system, the effect of using different applied hydraulic pressures for the two modules is investigated. From a thermodynamic perspective, reducing hydraulic pressure in the second module reduces entropy generation and increases power density. The single stage systems use the membrane unevenly, with most fresh water drawn early close to the inflow, and only little drawn further downstream.

To model the system, mass and momentum balances are formulated. To illustrate the configurations, sea water is considered as the draw solution and distilled water as the feed solution, other solutions could be considered as well. To quantify the system performance, hydraulic pressures and inlet flows of draw and feed solutions play an important role. These variables need to be obtained through an optimization procedure which depends on target functions. For this purpose, several functions are used: (a) power output per membrane area, (b) power per inlet draw and feed solutions, and (c) power per amount of fresh water drawn through the membrane. The functionality and necessity of these target functions are described, and the optimum values for applied hydraulic pressures as well as draw and feed inlet flow rates are obtained in order to maximize each work regime. The single and dual stage systems are compared in terms of target functions for optimization and thermodynamic analysis. The variation of some parameters through the membrane elements is compared between single and dual stage systems.

2. Methodology

2.1. General

In the current study, large scale dual stage PRO systems with new configurations are presented and compared to a single stage system. Fig. 1 presents several configurations of both single and dual stage PRO systems. Schematic diagrams of a simple single stage PRO system and a dual stage PRO both equipped with pumps and turbines are shown in Fig. 1 (a) and (b), respectively. These simple models are presented to be compared with PRO systems that employ pressure exchangers (PX) in order to obtain efficiency improvement, as shown in Fig. 1 (c) to (g).

Two configurations of dual stage PRO systems with PX and two Hydro-Turbines (HT) are proposed in Fig. 1 (d) and (e). The effects of applying various hydraulic pressures to each module are investigated after addition of the second hydro-turbine. Thermodynamically, depressurizing the draw solution before entering the second module may reduce the entropy generation by more even utilization of membrane through the channel.

To compare the dual stage systems with single stage ones Fig. 1 (c) and to find out the effect of adding the second turbine Fig. 1 (g) are presented. To find out the effect of exchanging the high pressure pump with the second PX, the configuration of Fig. 1 (f) is also proposed.

Many different configurations for dual stage PRO employing pressure exchangers, pumps and turbines are possible, and a detailed analysis based on thermodynamic modeling is required to evaluate the merits and failures of the different configurations. It is noted that more complex models might increase the capital cost, while providing savings in operation. For the subsequent analysis, optimization based on operating cost, not capital cost, is considered.

The length of the membrane for the single stage module is twice the length for each module in the dual stage system; i.e., $L_1 = L_2 = L/2$, where L is membrane length for the single stage module, and L_1 and L_2 are membrane length of first and second modules in a dual stage system, respectively. In terms of capital cost, dual stage PRO modules may need more membrane area in comparison with the single stage PRO systems. However, the same membrane area is used for all configurations presented in the current research.

In the counter-current flow through a module, draw and feed solutions have the opposite flow directions. As elaborated by van der Zwan et al. [21], the counter-current flow gives an approximately 15% higher power output compared to co-current flow. The higher production of power under counter-current flows in PRO systems is due to the more even distribution of salinity. Considering this, all suggested PRO configurations in this research have been studied in the counter-current flow direction.

The efficiency study of the basic single stage and dual stage PRO systems (Fig. 1 (a) and (b)) is followed by evaluation of the other proposed configurations, as shown in Fig. 1 (c) to (g). The proposed configurations employ high pressure pumps (HP), booster pumps (BP), PRO membrane modules, hydro-turbines (HT), and in the case of Fig. 1 (c) to (e) pressure exchangers (PX). The efficiencies of these pumps, turbines and PX play an important role for the overall system performance.

For an ideal pump and turbine system, the isentropic efficiencies are $\eta_P = \eta_T = 1$, where η_P and η_T denote pump and turbine efficiencies, respectively. In practice, these values are typically around 0.9. The current study is conducted assuming realistic efficiencies for all pumps and turbines.

For pressure exchangers, as explained by Bharadwaj et al. [22], in the relevant pressure ranges of PRO systems, pressure losses for high pressure stream (δP_H) and low pressure stream (δP_L) are approximately $\delta P_H = \delta P_L = \delta P = 0.5$ bar. These pressure losses are atoned by booster pumps in the configurations of Fig. 1.

In the dual stage system of Fig. 1 (b), the entering volumetric flow of the draw solution ($Q_{D,in}$) has environmental pressure at P_0. After

pressurizing to P_{D1}, the flow runs along a semipermeable membrane drawing the fresh water flux $Q_{drawn1} = \int J_{wr1} dL_1$. In this equation, J_{wr1} is fresh water drawn through the membrane from feed to draw solution. The outlet flow from module 1 (Q_{DL}) is equal to $Q_{D,in} + Q_{drawn1}$. Due to friction and flow resistance along the membrane, the pressure will drop from P_{D1} to P_{DL} upon exiting the first module. The flow drives the first turbine (HT1) and depressurizes to P_{D2}. At this point, the flow enters the second module at pressure P_{D2} and volumetric flow Q_{DL}. The same procedure happens in module 2, resulting in the exiting volumetric flow $Q_{DL,2} = Q_{D2} + Q_{drawn2}$, with $Q_{drawn2} = \int J_{wr2} dL_2$, where J_{wr2} is defined for module 2 similar to J_{wr1}. Similar to the process in module 1, the pressure will decrease to $P_{DL,2}$. The flow will drive the second turbine (HT2) and discharge to the environmental pressure P_0.

A single stage PRO equipped with a PX is shown in Fig. 1 (c). The PX is added to improve the efficiency of the system. In this configuration, a PX is used to pressurize the draw solution with the flow rate of $Q_{D,in}$ from P_0 to P_{D1} - δP. The internal head loss δP in PX and the frictional pressure drop in the membrane modules are compensated by booster pumps (BP) before the flow enters the module and on the way back to PX, respectively. At the end of the module, the flow splits into Q_{drawn} which runs the HT, and $Q_{D,in}$, which is sent back to the PX, where it is depressurized.

A dual stage PRO system equipped with a PX is shown in Fig. 1 (d). The PX pressurizes the inlet flow from P_0 to P_{D2}. Following this stage, an HP pressurizes the flow to P_{D1}. Then, the flow enters the first module and exits with volumetric flow Q_{DL}. The fluid is depressurized to P_{D2} following the passage through HT1 and then enters to module 2. The outlet fluid from module 2 is divided into two parts. The first part returns to PX with volumetric flow $Q_{D,in}$. The second part enters to HT2 with volumetric flow Q_{Drawn}($= Q_{Drawn1} + Q_{Drawn2}$).

In a dual stage PRO, the flow returning to the PX can be deviated after the second module or the first module, as shown in Fig. 1 (d) and (e), respectively. In the latter case (Fig. 1 (e)), a PX pressurizes the draw solution from P_0 to P_{D1} - δP to enter the first module. The exiting flow from the first module is divided into $Q_{D,in}$ (back to PX) and Q_{drawn1} (entering to the second module). Q_{drawn1} runs HT1 while depressurizing to P_{D2} and enters the second module. The exiting flow from the second module Q_{drawn} runs the HT2 while depressurizing to P_0. The booster pumps compensate the internal head loss δP in PX and the frictional pressure drop in the membrane modules.

A considerable improvement in system efficiency is anticipated after replacing the HP from Fig. 1 (a) and (b) with PX in Fig. 1 (d) and (e). In Fig. 1 (d) and (e) the difference in the applied pressure between two modules (P_{D1} and P_{D2}) is provided by a HP. If the difference between P_{D1} and P_{D2} is sufficiently large, this HP can also be replaced with a second PX. In order to investigate the efficiency of adding another PX instead of the HP, the configuration shown in Fig. 1 (f) is proposed. In this configuration, the HP is substituted by the second PX. The first PX pressurizes the flow from P_0 to P_{D2}, and the second one pressurizes it from P_{D2} to P_{D1}. The exit flow from module 1 splits into the two streams $Q_{D,in}$ and Q_{drawn1}. The $Q_{D,in}$ returns to the second PX at pressure of P_{D1} and leaves at P_{D2}. The flow at volumetric rate Q_{drawn1} drives the first turbine. Following the combination with the depressurized flow $Q_{D,in}$, the flow enters the second module at pressure P_{D2}. After the second module, the diluted draw solution is divided into the flows at volumetric flow rates $Q_{D,in}$ and Q_{drawn}. The former returns to the first PX and the latter drives the second turbine.

The last configuration is shown in Fig. 1 (g). The effect of having two counter-current feed flows for each module is investigated. In this configuration, [18], the draw flow after the first module is not depressurized - i.e., there is no HT1. The draw solution with a volumetric rate of $Q_{D,in}$ at pressure of P_0 is pressurized by a PX to P_{D1} and enters module 1. Then it runs into the second module at the pressure of $P_{DL,1}$. The exiting flow is split between $Q_{D,in}$ and Q_{drawn}. $Q_{D,in}$ returns to PX. The remaining flow at Q_{drawn} drives the HT.

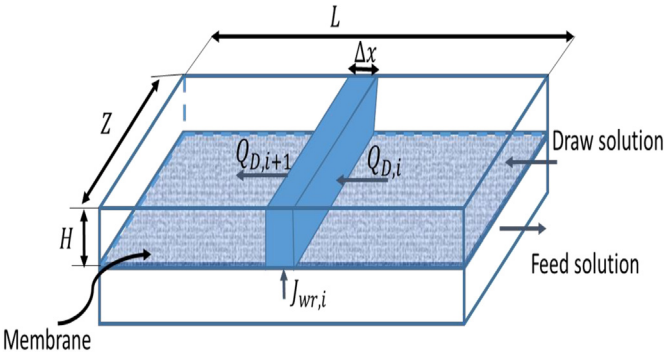

Fig. 2. Volumetric slice of the draw channel with thickness of Δx, height of the channel (H) and width of the channel (Z).

2.2. Mass balances of water and solutes in membrane

The study of flow through a membrane is achieved by application of conservation laws. Assuming a constant temperature, thermal effects can be ignored. Therefore, the conservation laws are simplified to mass and momentum balances.

As shown in Fig. 2, the volume of a slice of salt water with thickness dx is $V = \int HZdx$, where height of the channel (H) and width of the channel (Z) are given values. Integration of flow over the volume of a slice of salt water will have the compact form

$$\frac{dQ_D}{dx} = -\frac{dQ_F}{dx} = J_{wr}, \tag{1}$$

where J_{wr} is the water flux passing through the membrane, and dQ_D and dQ_F are the flow rate differential in the draw and feed solutions, respectively. The difference in signs is related to the difference in current direction.

In an ideal semipermeable membrane, salt does not pass through the membrane and the water flux passing through is generally described by Baker [23]

$$J_{wr} = A(\Delta\pi - \Delta P) = A(\pi_D - \pi_F - \Delta P), \tag{2}$$

where A is the water permeability, π_D and π_F are bulk osmotic pressures in draw and feed solutions, respectively, and $\Delta\pi = \pi_D$ - π_F. ΔP is the applied hydraulic pressure difference between the two flows. By considering both feed and draw solutions as incompressible liquids and sufficiently diluted, the van't Hoff equation can be used to approximate the osmotic pressures as

$$\pi = ic\bar{R}T. \tag{3}$$

In this expression i is the van't Hoff factor which represents the degree of dissociation, c is the molar concentration of salt, $\bar{R}$ is the universal gas constant, and T is the thermodynamic temperature of the solution. In the draw solution, 1 l of sea water typically consists of 35 g NaCl which dissociates into Na^+ and Cl^- ions ($i = 2$), and 993 g of fresh water. Hence, the molar concentration of salt in the draw solution is $c_D = 600$ mol. At a temperature of 298 K, the osmotic pressure of the draw solution is $\pi_D = 29.7$ bar [24]. Since the concentration of salt in the incoming feed solution is considered zero, the osmotic pressure of the incoming feed solution is $\pi_F = 0$.

Eq. (2) is only valid for an ideal membrane. In practice, the equation needs to be modified. For this purpose, the following need to be considered in the equation (see Fig. 3):

1. Reverse salt flux (RSF);
2. Internal concentration polarization (ICP); and
3. External concentration polarization (ECP).

RSF occurs due to non-selective behavior of membranes. Hence, salt permeates from the draw solution to the feed solution in the opposite

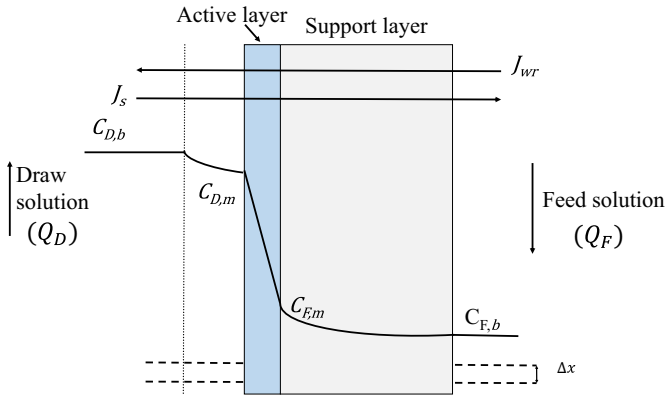

Fig. 3. A schematic of salt concentration profile in a membrane module. The modeling is forward for both draw and feed solutions.

direction of water permeation. RSF is described by [25]

$$J_s = B(c_{D,m} - c_{F,m}) \tag{4}$$

where J_s is the reverse salt flux, B is the salt permeability coefficient, and $c_{D,m}$ and $c_{F,m}$ are the solute concentration right at the membrane in draw and feed sides, respectively. Mass conservation law for reverse salt flux (molar flux) is the change of salt flow ($d(Q_c)$) in the element of dx, where c_F and c_d are the concentration of dissolved salt in feed and draw solutions, respectively:

$$J_s = \frac{d(Q_F c_F)}{dx} = -\frac{d(Q_D c_D)}{dx}. \tag{5}$$

The concept of ICP describes the accumulation of salt in the support layer facing the feed side. This acts as an unstirred boundary layer and increases the feed osmotic pressure π_f. As a result, the transmembrane driving force is reduced.

ECP mainly happens on the draw solution side. The fresh water coming through the membrane needs to be mixed with the more concentrated draw solution. The driving force for the fresh water is osmotic pressure at the membrane where the fresh water arrives. In the absence of perfect mixing in the draw channel, the local osmotic pressure and, hence, the driving force will decrease drastically. Therefore, the energy extraction in this process will attenuate. Solving Fick's first law for J_s is proceeded by introducing the structural parameter (S) as an effective diffusion coefficient. S is defined as $\frac{D\varepsilon}{\tau}$ where D is the diffusion coefficient of the draw solute in the porous support, ε is porosity, and τ is tortuosity [26]. Integration over the support layer thickness yields the effective salt and water flux [26]

$$J_{wr} = A\left\{\frac{\pi_D e^{\frac{-J_{wr}}{k}} - \pi_F e^{\frac{J_{wr}S}{D}}}{1 + \frac{B}{J_{wr}}[e^{\frac{J_{wr}S}{D}} - e^{-\frac{J_{wr}S}{k}}]} - \Delta P\right\}, \tag{6}$$

$$J_S = B\left\{\frac{c_D e^{\frac{-J_{wr}}{k}} - c_F e^{\frac{J_{wr}S}{D}}}{1 + \frac{B}{J_{wr}}[e^{\frac{J_{wr}S}{D}} - e^{\frac{-J_{wr}S}{k}}]}\right\}. \tag{7}$$

Some other models have been developed considering $C_{F,m} \neq C_{F,b}$ and $k_F \neq k_D$ for flat sheet membranes which include the external salt resistance in feed solution as well as draw solution [27,28]. However, the ECP effect in feed solution has been ignored in this study since the selected feed solution concentration is zero and the salt permeability in the selected membrane is at the low-end. For future studies with a wider variety in the draw and feed solution sources and membrane characteristics, the presented model will consider the external salt resistance in feed solution.

Other than being widely used in PRO system modeling [8,29,30], this model has been used in evaluating the dual stage system performance by other research groups [31,32]. It also has been used for modeling scaled up PRO systems [20,33,34]. The model is considered to be relatively accurate and has been validated by experiments for flat sheet membranes [26,35,36]. As an example, a comparison by Altaee et al. [36] showed 6% deviation of the model and the experimental data from [37]. In PRO modules, the model has been validated for both spiral wound [38] and hollow fiber membrane modules [39,40]. The model, accepted to be valid, has also been used in experimental studies to find the structural parameter in spiral wound membrane modules [41].

2.3. Momentum balance

The pressure losses in the membrane modules are determined from the balance of the momentum. Pressure loss is caused by friction in the channel and is related to the size of the channel, and the flow rates, and the friction factor. Similar to mass balance, diffusion due to variation in composition variation of the solution is ignored and thermal effects are ignored. Integration over a slice of salty water of volume dV, the momentum balance equation assumes the form

$$\int_V \frac{\partial(\rho v_i v_k + P\delta_{ik} - \sigma_{ik})}{\partial x_k} dV = 0, \tag{8}$$

where ρ is the mass density of the flow, v_i is the flow velocity, P is the pressure, and σ_{ik} are viscous stresses. Considering $V = HZdx$ (see Fig. 2) and applying the Gauss theorem

$$\int_{\partial V} \partial(\rho v_i v_k + P\delta_{ik} - \sigma_{ik}) n_k dA = 0, \tag{9}$$

where ∂V is the surface of V, and n_k is the outward normal. Since there are no boundry effects along z direction, the longitudinal component for the momentum equation is

$$Z\int_{-H/2}^{H/2} [\rho(x+dx,y)v_x^2(x+dx,y) - \rho(x,y)v_x^2(x,y)dy]dy + HZ[P(x+dx) - P(x)] - \int_{\partial V} \sigma_{xk} n_k dA = 0, \tag{10}$$

In Eq. (10), considering a plug flow condition, the volumetric flow rate in x direction is $Q_x = \frac{Q}{HZ}$. By averaging the first term, Eq. (10) turns to

$$\frac{1}{HZ}\frac{d(\rho Q^2)}{dx}dx + HZ\frac{d\Delta P}{dx}dx = \int_{\partial V} \sigma_{xk} n_k dA, \tag{11}$$

where Q is the average volumetric flow along the membrane. Integrating the above equation over the surface Zdx when side forces are ignored, gives

$$\frac{1}{HZ}\frac{d(\rho Q^2)}{dx} + HZ\frac{d\Delta P}{dx} = Z\sigma_{xy}^w, \tag{12}$$

where σ_{xy}^w is the average surface stress at the membrane. The Darcy friction factor f is defined as

$$f = \frac{8\,|\sigma_{xy}^w|}{\rho v^2}, \tag{13}$$

so the momentum equation can be written as

$$\frac{d(\rho Q^2)}{dx} + (HZ)^2\frac{d\Delta P}{dx} = -\frac{f_{mix}}{8}\frac{\rho Q^2}{H}, \tag{14}$$

f_{mix} is the modified friction factor in the presence of spacers [42].

2.4. Mass transfer and frictional pressure drop

For proper operation of the system, it is essential that the freshwater entering the draw side through the membrane is effectively mixed with the saltwater. In this way, the salt concentration is homogenous along y direction at x. Indeed, the driving force for the freshwater is related to

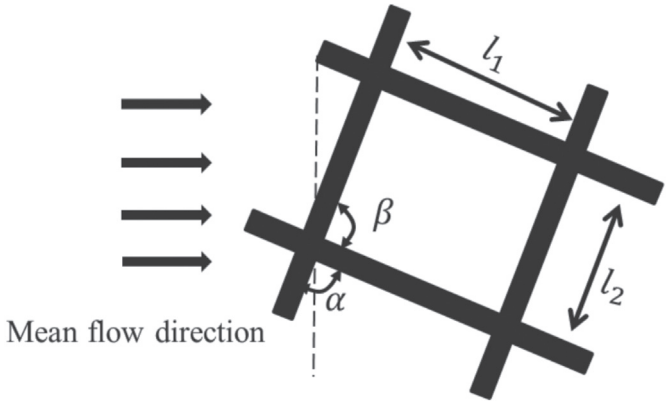

Fig. 4. The geometric parameters of a non-woven spacer.

the osmotic pressure at the location where the freshwater passes through the membrane. If the newly arrived freshwater is not mixed effectively, the local osmotic pressure and eventually the driving force are decreased drastically. Hence, successful mixing is imperative for proper operation.

The effective mixing can be achieved by introducing spacers into the channel. Indeed, spacers have a dual function of providing mechanical support for the membranes and being vortex promoters in channels. Spacers induce more flow resistance due to the increased friction. CFD studies on flow patterns near obstacles show spiral and erratic motions [43,44].

In comparison to laminar flow, the existing flow regime has more flow resistance, due to an additional irreversibility. In this condition, there is an interaction between the pressure drop due to friction and an improvement of mass transportation (mixing). The former decreases the net work, while the latter increases it. To find the best performance, it is necessary to optimize the spacers' configuration. Schock and Miquel [45] measured mass transfer and flow resistance in flat channels and spiral wound modules filled with various commercial spacers. In the current study, a simple geometry of non-woven net spacers is considered. The relation between the mass transfer and power dissipation (in terms of pressure losses) is attained by using the results obtained from Li et al. [46]. These results have been validated with experiments in spiral wound membrane modules and as shown in [46], the simulations are in good agreement with the experiments.

The spacer geometrical parameters include the distance between spacer filaments $l_1 = l_2$, where $l = l_1 + l_2$, angle between the spacer filaments β, channel height H, and flow attack angle α as in Fig. 4.

Li et al. [46] found the optimum geometrical values as $H/l = 4$, $\alpha = 30^\circ$, and $\beta = 120^\circ$. They introduced a dimensionless power number P_n which is the normalized value of pressure drop in the channel which is correlated with Reynolds number (Re). Moreover, it can be related to the Sherwood number (Sh) which is related to effective diffusion coefficient (d). Considering the relations between the aforementioned parameters, it is possible to show the effect of changes in Reynolds number as a turbulence factor and the trade-off between pressure drop due to friction and enhancing mass transport.

For a wide channel, where side effects can be ignored ($Z >> H$), the hydraulic diameter is $D_H = 2H$, and the Reynolds number is

$$Re = \frac{D_H \rho v}{\eta} = \frac{2H\rho v}{\eta} = \frac{2Q}{\nu}, \tag{15}$$

where $\nu = 1.57 \times 10^{-6}$ m^2/s is the kinematic viscosity. In [46], the following contributions are found,

$$P_n = 5Re^{2.6}, \tag{16}$$

$$Sh = 2.5P_n^{0.25}, \tag{17}$$

the Sherwood number is defined as

Table 1
Parameters used in PRO model.

Model parameters	Values
Water permeability, A [m s^{-1}Pa^{-1}]	4.86×10^{-12} [33]
Salt permeability, B [m s^{-1}]	4.44×10^{-8} [33]
Structural parameter, S [m]	307×10^{-6} [33]
Temperature, T[K]	298
Diffusion coefficient of salt, D [m^2 s^{-1}]	1.49×10^{-9} [33]
Draw solution concentration, c_D [mol m^{-3}]	600
Feed solution concentration, c_F [mol m^{-3}]	0
Mass transfer coefficient, k [m s^{-1}]	3.85×10^{-5} [33]
Membrane length, L [m]	15 for single module, 7.5 for dual stage modules
Membrane width, Z [m]	1
Flow channel height, H [m]	0.001
Pump, turbine efficiency	0.9

$$Sh = \frac{kH}{d}, \tag{18}$$

k is the mass transfer coefficient for the membrane and d is the effective diffusion coefficient. The friction factor is:

$$f_{mix} = \frac{p_n}{Re^3} = 5Re^{-0.4}, \tag{19}$$

Considering Eqs. (16) to (19) and Eq. (14) the pressure drop along the channel is known and the balance of momentum becomes

$$\frac{(\rho Q^2)}{dx} + (HZ)^2 \frac{d\Delta P}{dx} = -\frac{Pn}{8Re^3}\frac{\rho Q^2}{H}. \tag{20}$$

The improvement in mass transfer is achieved by updating d value along the module.

2.5. PRO modeling

The inlet volumetric flow of draw (Q_D) and feed solutions (Q_F), as well as hydraulic pressures of the first (P_{D1}) and the second (P_{D2}) module are variable parameters which must be optimized in order to find the maximum power output.

The selection of membrane parameters appropriate for PRO was studied in detail by Wang et al. [47]. However, most PRO membranes are on laboratory scale and still need to be tested on larger scales.

The selected parameters in this paper are listed in Table 1. Some of the selected parameters are based on the values presented by Wei et al. [33].

The governing equations for counter-current flow are obtained from Eqs. (1) to (7). The mass transfer of water and salt fluxes in Eqs. (6) and (7) needs to be solved for a differential element. Then, the results need to be related to changes in water flow rates and solute concentrations based on mass balance in Eqs. (1) and (5). Hence, on both, the draw and feed sides, water flux (J_{wr}) is expressed in Eqs. (1) and (2) and the reverse salt flux (J_s) equation is expressed in Eqs. (4) and (5). The updates for the pressure drop is obtained from Eq. (20) and the mass transfer coefficient is updated by updating Eqs. (6) and (7) with Eq. (18).

The volumetric flow rates, osmotic and hydraulic pressures, salt concentrations and mass transfer in both draw and feed solutions are updated by marching along the membrane with $\Delta x = \frac{L}{n}$ where n is the number of grid points. The marching is at the same direction in both draw and feed channels. Considering the counter-current flow in the channels, the boundary conditions are different in each channel. For module 1, the initial values for volumetric flow rates are $Q_D(0) = Q_{D,in}$, $Q_F(0) = Q_{F,in}$, where $Q_{D,in}$ and $Q_{F,in}$ are the selected inlet volume flow rates of draw and feed solutions, respectively. The initial salt concentrations in draw and feed solutions are $c_D(0) = c_{D,in}$, $c_F(0) = 0$. For module 2, the inflow conditions become $Q_D(0) = Q_{D,L}$, $Q_F(0) = Q_{F2,in}$ where $Q_{D,L}$ is the exiting flow rate from module 1 and $Q_{F2,in}$ is the selected inlet volume flow rate of feed solution in module 2. For solute

concentration the inflow conditions are $c_D(0) = c_{D,L}$, $c_F(0) = 0$, where $c_{D,L}$ is the concentration of salt at the end of module 1 in the draw solution.

2.6. Quantifying the system performance

For the system with pump and turbine, the general power equations for pump and turbine are

$$\dot{W}_P = \frac{1}{\eta_P} Q(P_{in} - P_{out}) < 0, \tag{21}$$

$$\dot{W}_T = \eta_T Q(P_{in} - P_{out}) > 0, \tag{22}$$

where $\dot{W}_P$ and $\dot{W}_T$ are the power required to pressurize or obtained from depressurizing in pump and turbine, respectively, and Q is the volumetric flow rate. P_{in} and P_{out} are input and output pressures, respectively. Net power output is the sum of pump and turbine powers,

$$\dot{W}_{net} = \dot{W}_T + \dot{W}_P. \tag{23}$$

As shown in Fig. 1, seven different configurations are suggested. Power outputs corresponding to each configuration are presented in Eqs. (24) to (31).

For the single stage system equipped with pump and turbine (Fig. 1 (a)), the power output is

$$\dot{W}_{net} = \eta_T Q_{DL}(P_{DL} - P_0) - \frac{1}{\eta_P} Q_{D,in}[(P_{D1} - P_{DL}) + Q_{F,in}(P_{F1} - P_0)], \tag{24}$$

For the dual stage system equipped with pump and turbine (Fig. 1 (b)), the power output is

$$\dot{W}_{net} = \eta_T [Q_{DL}(P_{DL} - P_{D2}) + Q_{DL,2}(P_{DL,2} - P_0)] - \frac{1}{\eta_P}[Q_{D,in}(P_{D1} - P_0 + Q_{F1,in}(P_{F1} - P_0) + Q_{F2,in}(P_{F2} - P_0)], \tag{25}$$

In the presence of PX, the required work for booster pumps to compensate the pressure loss of PX ($\delta\dot{W}_{PX}$) is

$$\dot{W}_{PX} = Q_{D,in}(\delta P_H + \delta P_L) = 2Q_{D,in}\delta P, \tag{26}$$

For the single stage system with the pressure exchanger (Fig. 1 (c)), the power output is

$$\dot{W}_{net} = \eta_T Q_{drawn}(P_{DL} - P_0) - \frac{1}{\eta_P}[Q_{D,in}(2\delta P + (P_{D1} - P_0)) + Q_{F,in}(P_F - P_0)], \tag{27}$$

For the dual stage system with 1 pressure exchanger (1PX) shown in Fig. 1 (d), the power output is

$$\dot{W}_{net} = \eta_T [Q_{DL}(P_{DL} - P_{D2}) + Q_{drawn}(P_{DL,2} - P0)] - \frac{1}{\eta_P}[Q_{D,in}((P_{D1} - P_{DL2}) + 2\delta P) + Q_{F1,in}(P_{F1} - P_0) + Q_{F2,in}(P_{F2} - P_0)], \tag{28}$$

For the dual stage system with (1PX) that drives back to the PX before the first HT (Fig. 1 (e)), the power output is

$$\dot{W}_{net} = \eta_T [Q_{Drawn1}(P_{DL} - P_{D2}) + Q_{drawn}(P_{DL,2} - P0)] - \frac{1}{\eta_P}[Q_{D,in}((P_{D1} - P_{DL}) + 2\delta P) + Q_{F1,in}(P_{F1} - P_0) + Q_{F2,in}(P_{F2} - P_0)], \tag{29}$$

For the dual stage system with 2 pressure exchangers (2PX) showed in Fig. 1 (f), the power output is

$$\dot{W}_{net} = \eta_T [Q_{Drawn1}(P_{DL} - P_{D2}) + Q_{drawn}(P_{DL,2} - P_0)] - \frac{1}{\eta_P}[Q_{D,in}(P_{D1} - P_{DL} + P_{D2} - P_{DL2} + 4\delta P) + +Q_{F1,in}(P_{F1} - P_0) + Q_{F2,in}(P_{F2} - P_0)], \tag{30}$$

Finally, for the dual stage system with 1PX and 1HT (Fig. 1 (g)), the power output is

$$\dot{W}_{net} = \eta_T [Q_{Drawn}(P_{DL2} - P_0)] - \frac{1}{\eta_P}[Q_{D,in}((P_{D1} - P_{DL2}) + 2\delta P) + Q_{F1,in}(P_{F1} - P_0) + Q_{F2,in}(P_{F2} - P_0)], \tag{31}$$

2.7. Target functions for optimization

Considering Eqs. (21) and (22), power output depends on pressures and volumetric flow rates. Therefore, they have to be chosen in order to achieve an optimum system performance. Based on the application, there are several methods to optimize the system performance. Note that the goal of all these methods is to make PRO economically feasible. To achieve this goal, most previous research has focused on optimizing for power density (*PD*) or specific energy (*SE*).

Power density is defined as the extractable work per membrane area [8],

$$PD = \frac{\dot{W}_{net}}{A_m}, \tag{32}$$

where $\dot{W}_{net}$ is the system power output and A_m is the total membrane area. Power density reflects the importance of membranes in PRO systems. Consideration of capital cost for the membrane and its partial maintenance cost is the rationale behind the consideration of the PD. Hence, the efficiency and utilization of membrane area are of great importance. Optimizing the *PD* results in smaller membrane area and obtaining higher power output per membrane area.

The second target function is specific energy (SE) which is defined as extracted energy per inlet flow rates of draw and feed solutions.

$$SE = \frac{\dot{W}_{net}}{Q_{F,in} + Q_{D,in}}, \tag{33}$$

$Q_{F,in}$ and $Q_{D,in}$ are inlet volumetric flow rates of feed and draw solutions, respectively. For dual stage PRO systems, $Q_{F,in} = Q_{F1,in} + Q_{F2,in}$, where $Q_{F1,in}$ and $Q_{F2,in}$ are inlet flow rates of feed solutions in the first and second module, respectively. Specific energy should be considered when the energetic costs of pumping and water pretreatment are important or the accessible amounts of draw and fresh water are restricted. The cost of pretreatment and pumping will increase with increasing the flow of water on each side of the membrane. *SE* can be used as an indicator of energy efficiency for the system.

Since optimization is based on the availability of fresh water rather than salt water, the optimization process can also be conducted based on drawn freshwater along the module. Hence, the extracted work per liter of drawn fresh water is defined as

$$W_{drawn} = \frac{\dot{W}_{net}}{Q_{drawn}}, \tag{34}$$

Each of the above descriptions is used as a target function for optimization, while P_{D1}, P_{D2}, $Q_{F1,in}$ and $Q_{F2,in}$ are variable parameters.

2.8. Thermodynamic analysis of PRO system

The Gibbs free energy of mixing is the thermodynamic upper bound of the energy. The maximum extractable energy of mixing two solutions with different salinities can be attained via a thermodynamically reversible process. A thermodynamically reversible process in the PRO system can be conducted by keeping the applied hydraulic pressure

infinitesimally below the osmotic pressure.

In general, the work supplied to the plant can be obtained from the Gibbs free energy of mixing, $\Delta\dot{G}$,

$$\dot{W} = -T\dot{S}_{gen} - \Delta\dot{G}, \tag{35}$$

where T is temperature, $\dot{S}_{gen}$ is entropy generation, and $\Delta\dot{G}$ is the Gibbs free energy per unit time. Any generation of entropy due to irreversible process reduces the work output.

Assuming an ideal mixture, the Gibbs free energy of mixing is

$$\Delta\dot{G} = \bar{R}T\sum_{out}\dot{n}_\alpha X_\alpha ln(X_\alpha) - \sum_{in}\dot{n}_\alpha X_\alpha ln(X_\alpha), \tag{36}$$

where $\bar{R}$ is the universal gas constant, $\dot{n}_\alpha$ is the mole flow of component α, X_α is the corresponding mole fraction. For reversible work, $\dot{S}_{gen} = 0$ and considering draw and feed solution Eq. (35) gives

$$\begin{aligned}\dot{W}_{rev} = & -\Delta\dot{G} = \bar{R}T\,[\dot{n}_D^{in}X_D^{in}ln(X_D^{in}) + \dot{n}_D^{in}(1-X_D^{in})ln(1-X_D^{in}) \\ & + \dot{n}_F^{in}X_F^{in}ln(X_F^{in}) - (\dot{n}_D^{out}X_D^{out}ln(X_D^{out}) \\ & + \dot{n}_D^{out}(1-X_D^{out})ln(1-X_D^{out}) \\ & + \dot{n}_F^{out}X_F^{out}ln(X_F^{out}) + \dot{n}_F^{out}(1-X_F^{out})ln(1-X_F^{out}))],\end{aligned} \tag{37}$$

where D and F indicate draw and feed solutions, respectively. Since $X_F^{in} = X_F^{out} = 1$, and assuming a dilute solution at both the draw and feed sides, Eq. (37) can be simplified to

$$\begin{aligned}\dot{W}_{rev} = -\Delta\dot{G} = i\bar{R}T\,[&\dot{n}_{D^{in}}X_D^{in}ln(X_D^{in}) - \dot{n}_{D^{out}}X_D^{out}ln(X_D^{out}) \\ & - \dot{n}_{F^{out}}X_F^{out}ln(X_F^{out})],\end{aligned} \tag{38}$$

Assuming negligible contribution of solute to the volume of the solution and dividing Eq. (38) to the volume of mixed solution, the Gibbs free energy per volume of total mixed solution is achieved. The resulting quantity is obtained as a function of molar concentrations of the draw and feed solutions (c_D and c_F), as well as volumetric flow of salt and water in the draw and feed solutions (Q_D and Q_F)

$$\begin{aligned}\Delta\dot{G} = i\bar{R}T\,[&Q_{D,in}c_{D,in}ln(c_{D,in}) - Q_{D,out}c_{D,out}ln(c_{D,out}) \\ & - Q_{F,out}c_{F,out}ln(c_{F,out})],\end{aligned} \tag{39}$$

The total work loss then can be expressed as

$$\dot{W}_{loss} = \dot{W}_{rev} - \dot{W}_{net}. \tag{40}$$

The sources for irreversible energy loss in a PRO system with PX, pump and turbine can be listed as follows:

1. Water and salt transfer through the membrane;
2. Pressure drop in pressure exchanger;
3. Pressure drop along the membrane in both sides;
4. In pump; and
5. In turbine.

Work loss of water transfer in the module is

$$\dot{W}_{loss}^{water} = T\dot{S}_{gen}^{water}, \tag{41}$$

where T is the temperature and $\dot{S}_{gen}^{water}$ is the entropy generation due to water transfer. The entropy generation is

$$\dot{S}_{gen}^{water} = \int \sigma_{gen}^{water}dA, \tag{42}$$

where A is the membrane area and σ_{gen}^{water} is the entropy generation per membrane area, as

$$\sigma_{gen}^{water} = \frac{\dot{n}_v}{T}(\bar{\mu}_v^{\,D} - \bar{\mu}_v^{\,F}), \tag{43}$$

$\dot{n}_v$ is mole flow of water, $\bar{\mu}_v^{\,D}$ and $\bar{\mu}_v^{\,F}$ are chemical potential of water at draw and feed side, respectively.

$$(\bar{\mu}_v^{\,D} - \bar{\mu}_v^{\,F}) = \bar{V}_w(\Delta_P - \Delta\pi), \tag{44}$$

and,

$$\dot{n}_v = \int J_v dA, \tag{45}$$

where J_v is the mole flux which has the relation of $J_v = \frac{J_{wr}}{\bar{v}_w}$. Considering the Eqs. (41)–(45) the work loss for water is

$$\dot{W}_{loss}^{water} = \sum_{i=1}^{n} J_{wr}(\Delta P - \Delta\pi)\Delta x. \tag{46}$$

For the salt transfer through the membrane

$$\dot{W}_{loss}^{salt} = \sum_{i=1}^{n} J_s Rln(\frac{c_D}{c_F})\Delta x. \tag{47}$$

Work loss of pressure exchanger

$$\dot{W}_{loss}^{PX} = Q_{D,in}2\delta P. \tag{48}$$

Work loss of pressure drop in the membrane considering both draw and feed solutions

$$\dot{W}_{loss}^{mem} = \frac{Q_{F,in} + Q_{F,out}}{2}(P_{F,in} - P_0) + \frac{Q_{D,in} + Q_{D,out}}{2}(P_{D,in} - P_{D,out}). \tag{49}$$

Work loss of pump

$$\dot{W}_{loss}^{P} = \dot{W}_{irr}^{P} - \dot{W}_{rev}^{P} = \left(\frac{1}{\eta_P} - 1\right)\dot{W}_{rev}^{P}. \tag{50}$$

$$\dot{W}_{loss}^{P} = \left(\frac{1}{\eta_P} - 1\right)[Q_{D,in}(2\delta_P + (P_{D,in} - P_{D,out})) + Q_{F,in}(P_{F,in} - P_0)]. \tag{51}$$

Work loss of turbine

$$\dot{W}_{loss}^{T} = (1 - \eta_T)Q_{drawn}(P_{D,out} - P_0). \tag{52}$$

Table 2
Optimization results for single and dual stage modules for maximum power density (PD).

	Single stage	Dual stage	Single stage	Dual stage (with 2 HT)			Dual stage (with 1 HT)
	1PT (a)	2PT (b)	1PX (c)	1PX (d)	1PX (e) **(before T1)**	2PX (f)	1PX (g)
PD (Wm^{-2})	**2.19**	**2.22**	**2.87**	**2.96**	**2.78**	**2.56**	**2.98**
SE (KJ Lit^{-1})	0.25	1.12	0.27	0.15	0.15	0.14	0.15
W_{drawn} (KJ Lit^{-1})	0.65	0.59	0.96	0.92	0.87	0.79	0.94
P_{D1} (bar)*	12	12.5	15	15	15	17.5	15
P_{D2} (bar)	—	11.5	—	14.5	11	12	—
$Q_{D,in} \times 10^{-4}$ (m^2s^{-1})	0.6	0.8	0.8	0.9	0.9	0.8	0.9
$Q_{F,in} \times 10^{-4}$ (m^2s^{-1})	0.7	1	0.7	1	1.2	1	1.1
$Q_{F2,in} \times 10^{-4}$ (m^2s^{-1})	—	1	—	1	0.7	1	0.1

* The presented P_{D1}, P_{D2}, $Q_{D,in}$, $Q_{F,in}$ and $Q_{F2,in}$ are the optimized values for PD.

Table 3
Optimization results for single and dual stage modules for maximum specific energy (SE).

	Single stage	Dual stage	Single stage	Dual stage (with 2 HT)			Dual stage (with 1 HT)
	1PT (a)	2PT (b)	1PX (c)	1PX (d)	1PX (e) **(before T1)**	2PX (f)	1PX (g)
PD (Wm^{-2})	1.06	0.82	1.15	0.84	0.87	0.96	1.13
SE (KJ Lit^{-1})	**0.44**	**0.49**	**0.51**	**0.53**	**0.55**	**0.52**	**0.46**
W_{drawn} (KJ Lit^{-1})	0.88	0.95	1.14	1.04	1.09	1.02	1.14
P_{D1} (bar)*	13.0	16.5	15.0	17.5	16.0	18.5	15.0
P_{D2} (bar)	—	11.0	—	11.5	10.5	11	—
$Q_{D,in} \times 10^{-4}$ (m^2s^{-1})	0.14	0.08	0.15	0.08	0.09	0.09	0.15
$Q_{F,in} \times 10^{-4}$ (m^2s^{-1})	0.22	0.08	0.19	0.07	0.09	0.07	0.15
$Q_{F2,in} \times 10^{-4}$ (m^2s^{-1})	—	0.09	—	0.09	0.06	0.11	0.07

* The presented P_{D1}, P_{D2}, $Q_{D,in}$, $Q_{F,in}$ and $Q_{F2,in}$ are the optimized values for SE.

Total work loss is the sum of all work losses

$$\dot{W}_{loss} = \dot{W}_{loss}^{water} + \dot{W}_{loss}^{salt} + \dot{W}_{loss}^{PX} + \dot{W}_{loss}^{mem} + \dot{W}_{loss}^{P} + \dot{W}_{loss}^{T}. \quad (53)$$

Eqs. (35) to (53) will be used in Section 3.1.4 for thermodynamic analysis of the system performance.

3. Results and discussions

3.1. Single stage versus dual stage PRO system

Some dual stage PRO configurations have been studied previously [15,18]. However, to the best knowledge of the authors, none of them has considered the effect of changing hydraulic pressures after each module. Tables 2—4 compare maximum work values for target functions with their inlet draw and feed solution pressures and flow rates. The values for the applied hydraulic pressures (P_{D1} and P_{D2}) and inlet draw and feed flow rates ($Q_{D,in}$, $Q_{F,in}$, and $Q_{F2,in}$) were changed so that the maximum value for each target function is obtained.

3.1.1. Power density(PD)

Optimization for the maximum amount of power density (PD) for each configuration, results in the optimal values for pressures and flow rates shown in Table 2. The dual stage system with pump and turbine (2PT) has slightly higher PD compared to single stage 1PT. However, this amount is less than PD in single stage system with PX, since the lower efficiency of the pump has canceled the advantage of dual stage system. The dual stage system with 1HT and 1PX configuration has the maximum PD and shows a 36% improvement compared to the single stage PT, 34% over dual stage 2PT, and 3.8% over single stage PX. The improvement from the dual stage to the single stage systems derives from separated feed flows which maximize the difference in salt concentration. However, adding the second HT and depressurizing the draw flow after the first module is not effective and the system tends to minimize the pressure difference between two modules. The 0.5 bar difference in the applied pressure between two modules is due to the selected pressure discretization step in the model. When this step size vanishes, as in the dual stage with 1HT, PD value improves. To investigate the losses and their effects on the system performance, a thermodynamic analysis of the system is presented in Section 3.1.4, see Table 5.

Looking at flow rates for dual stage systems, the feed flow rates have been optimized separately for each stream. For PD, $Q_{F,in}$ is almost equally distributed between the two modules and $Q_{D,in}$ is equal or less than $Q_{F,in}$. For all dual stage systems with 1PX, the optimum applied hydraulic pressure approaches the value at $\frac{\Delta\pi_D}{2}$.

3.1.2. Specific energy(SE)

As shown in Table 3, maximum specific energy (SE) is found for the dual stage 1PX design (e). This configuration shows an improvement of about 8% with respect to the single stage 1PX, 12% to the dual stage 2PT and 25% to the single stage 1PT. Generally, in the dual stage PRO systems, the optimum pressure for the first module is above $\frac{\Delta\pi}{2}$ and for the second module is below $\frac{\Delta\pi}{2}$. This means that the maximum SE is obtained for individual optimum pressures for each module. It implies that depressurizing before the second module is helpful and reduces the irreversibility. This will be proved by thermodynamic analysis provided for SE as shown in Section 3.1.4, see Table 6.

3.1.3. Work per fresh water drawn(W_{drawn})

As shown in Table 4, in the case of the dual stage system with 1PX, work per fresh water drawn shows a 61% improvement with respect to the single stage PT, 47% compared to dual stage 2PT, and 2% compared to single stage PX. Similar to PD, depressurizing the flow after the first module does not have any benefit and the improvement is only related

Table 4
Optimization results for single and dual stage modules for maximum work per drawn water (W_{drawn}).

	Single stage	Dual stage	Single stage	Dual stage (with 2 HT)			Dual stage (with 1 HT)
	1PT (a)	2PT (b)	1PX (c)	1PX (d)	1PX (e) **(before T1)**	2PX (f)	1PX (g)
PD (Wm^{-2})	0.73	0.63	0.72	0.69	1.36	0.65	0.74
SE (KJ Lit^{-1})	0.32	0.18	0.22	0.96	0.19	0.95	0.11
W_{drawn} (KJ Lit^{-1})	**1.0**	**1.1**	**1.59**	**1.61**	**1.49**	**1.44**	**1.62**
P_{D1} (bar)*	17.0	19.5	24.0	24.0	22.0	24.5	24.0
P_{D2} (bar)	—	11.0	—	11.5	10.5	11	—
$Q_{D,in} \times 10^{-4}$ (m^2s^{-1})	0.14	0.1	0.27	0.23	0.33	0.15	0.27
$Q_{F,in} \times 10^{-4}$ (m^2s^{-1})	0.2	0.23	0.22	0.36	0.64	0.44	0.31
$Q_{F2,in} \times 10^{-4}$ (m^2s^{-1})	—	0.23	—	0.46	0.06	0.44	0.42

* The presented P_{D1}, P_{D2}, $Q_{D,in}$, $Q_{F,in}$ and $Q_{F2,in}$ are the optimized values for W_{drawn}.

Table 5
Thermodynamic analysis for single and dual stage modules for net work and losses percentages for PD.

	Single stage	Dual stage	Single stage	Dual stage			Dual stage
				(with 2 HT)			(with 1 HT)
	1PT (a)	2PT (b)	1PX (c)	1PX (d)	1PX (e) **(before T1)**	2PX (f)	1PX (g)
Net work %	29.61	25.33	39.6	37.16	35.22	33	38.01
Total work loss %	**70.39**	**74.66**	**60.4**	**62.84**	**64.78**	**66.97**	**61.99**
Water and salt transfer %	50.71	52.26	42.88	44.25	44.04	43.86	44.03
Pressure exchanger %	—	—	8.2	8.38	8.43	14.51	8.51
Turbine %	10.72	11.46	5.78	5.87	4.99	5.62	5.51
Membrane module %	2.33	3.16	3.55	3.91	3.93	2.98	3.94
Pump %	6.63	7.78	—	0.42	3.37	—	—

to the individual feed flows for each module.

It is worthwhile to note that using multi stage systems with additional stages will facilitate more energy recovery as discussed in [19]. However, it may not be economically feasible. As shown in Tables 2—4, achieving one optimized target function requires sacrificing the other. Therefore, the designer should be precisely aware of what the most important issue in each power plant is. For instance, the optimization for W_{drawn} requires high applied pressures which are far from the optimum values for PD or SE. Hence, the results for these target functions are very low, and might not be acceptable.

For all target functions, the values for dual stage 1PX 2HT are higher than the single stage. In the presence of incoming fresh water drawn through the membrane, the osmotic pressure in draw solution (π_D) decreases. Hence, according to Eq. (3), J_{wr} decreases along the module. One advantage of dual stage configurations is that by dropping the hydraulic pressure to a specific value half way, the pressure difference ($\Delta\pi$ - ΔP) will remain almost the same and the flux across the membrane (J_{wr}) will not change drastically. Another advantage of dual stage systems is that two separate fresh water streams for each module are used instead of one long stream. According to Eq. (3), the osmotic pressure of the feed solution (π_F) will decrease along the module due to contamination with the salt flow (J_s). Therefore, the fresh water inlet in the second module will increase the osmotic pressure difference. This increase in driving force helps to take more water in and may also increase the power output. This effect is more tangible with longer modules, where the fresh water is more concentrated at the terminal part of module.

In Fig. 1 (c) to (g), all configurations with PX produce more work than PT configurations which is predictable due to the higher efficiency of PX. However, for all target functions, the power produced with 2PX is equal or even less than the single stage PRO with 1PX. This means the addition of the second PX in Fig. 1 (e), does not improve efficiency. As discussed in [19], the best operation condition for PX is when it works for higher pressure differences. For smaller pressure differences similar to the case of dual stage PRO systems, pressure exchangers lose the advantage against pump-turbine pairs. Therefore, in the configuration of Fig. 1 (e) the pressure increase from P_{D1} to P_{D2} is not high enough to take advantage of the second PX. The pressure difference can better be obtained by a booster pump.

Interestingly, in cases where the difference between P_{D1} and P_{D2} is significant, the optimum applied hydraulic pressures for all target functions in single stage systems lie between the two optimum values of pressures in dual stage systems. This implies that in the dual stage systems, the application of optimal conditions of single stage module in the operation conditions will not meet the global maximum of the dual stage system.

3.1.4. Thermodynamic analysis of the PRO systems

Thermodynamic analysis is conducted based on the equations presented in Section 2.8. For each target function, the percentage of net work and total work loss is presented in Tables 5 to 7. As observed in the tables, except for PD, the percentile of the net work for the dual stage systems is more than for single stage systems. The reversible work in a dual stage system is expected to be more than a single stage system. For this reason, even though the amount of net work or power density in a dual stage system is more than a single stage in the case of PD, the losses of dual stage system exceed the improvement in net work. This results in decrease of percentile of net work in dual stage systems.

The maximum net work percentage of all target functions belongs to SE in the dual stage 1PX system where Q_{Din} is drawn back to PX before the first turbine Fig. 1 (e). This system also has the maximum improvement with respect to the single stage system. In this case, the pressure drop is significant and confirms that depressurizing the draw solution before the second module is beneficial. Drawing the Q_{Din} back to the PX after the first module causes more net work percentage in SE and W_{drawn} target functions. This is expected since Q_{Din} will eventually be send back to the PX and does not contribute to power production. The unnecessary losses resulting from Q_{Din} flow into the second module are avoided. However, the amount of W_{drawn} is larger in dual stage 1PX Fig. 1 (e) and Table 4) rather than the single stage 1PX system where Q_{Din} is drawn back to PX after the first module. This can be explained by the fact that, by the definition of W_{drawn}, the division of the amount of

Table 6
Thermodynamic analysis for single and dual stage modules for net work and losses percentages for SE.

	Single stage	Dual stage	Single stage	Dual stage			Dual stage
				(with 2 HT)			(with 1 HT)
	1PT (a)	2PT (b)	1PX (c)	1PX (d)	1PX (e) **(before T1)**	2PX (f)	1PX (g)
Net work %	44.96	51.67	53.77	55.45	56.70	56.08	52.85
Total work loss %	**55.04**	**48.33**	**46.23**	**44.55**	**43.30**	**43.92**	**47.15**
Water and salt transfer %	38.67	30.27	34.15	29.01	29.72	29.31	35.18
Pressure exchanger %	—	—	5.19	3.89	4.3	7.39	5.19
Turbine %	10.72	11.46	5.78	5.87	4.99	5.62	5.51
Membrane module %	10.82	12.17	6.58	9.20	6.78	7.1	6.47
Pump %	0.32	0.11	0.31	0.1	0.11	0.12	0.3

Table 7
Thermodynamic analysis for single and dual stage modules for net work and losses percentages for W_{Drawn}.

	Single stage	Dual stage	Single stage	Dual stage (with 2 HT)			Dual stage (with 1 HT)
	1PT (a)	2PT (b)	1PX (c)	1PX (d)	1PX (e) **(before T1)**	2PX (f)	1PX (g)
Net work %	42.1 4	44.1	51.15	48.08	53.14	46.96	48.60
Total work loss %	**57.86**	**55.90**	**48.85**	**51.92**	**46.59**	**53.04**	**51.04**
Water and salt transfer %	32.59	30.71	26.32	31.36	24.69	30.53	30.52
Pressure exchanger %	—	—	14.22	11.94	9.67	15.22	13.18
Turbine %	15.35	15.49	7.38	7.39	7.05	7.02	6.93
Membrane module %	0.33	0.18	0.93	0.63	0.35	0.27	0.76
Pump %	9.59	9.52	—	0.6	4.83	—	—

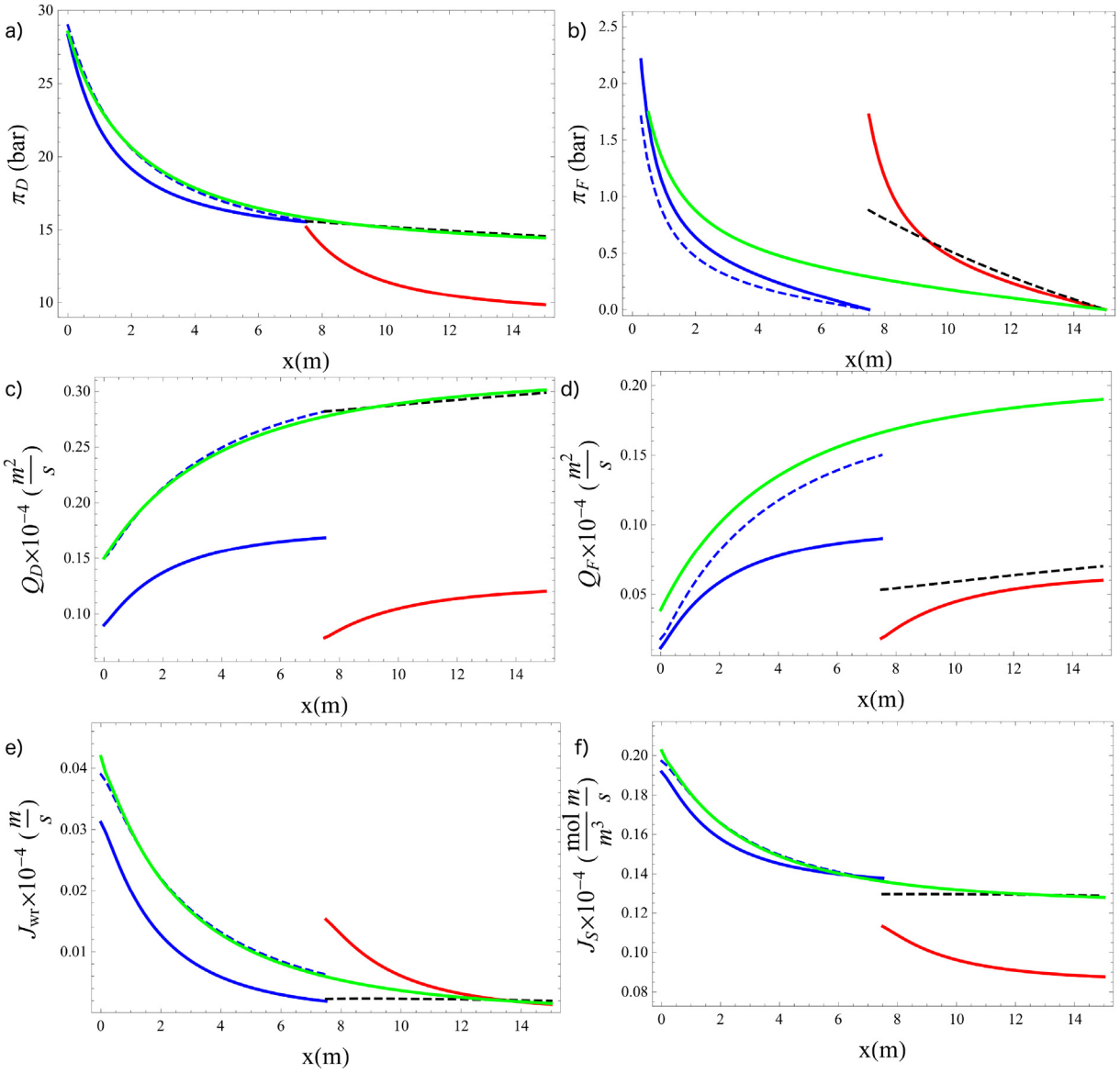

Fig. 5. Osmotic pressure of draw and feed solutions (a) and (b)(π_D,π_F); (c) and (d) volumetric flow rate of draw and feed solutions (Q_D,Q_F); (e) permeated water flux (J_{wr}) and (f) reverse salt flux (J_s), in the case of optimal power production in single and dual stage systems configuration (e) (blue line for module 1, and red line for module 2) and a dual stage system with 1HT (blue dashed line for module 1, and black dashed line for module 2) for the counter-current optimum values obtained for specific energy (SE).

net work to the inlet flow rate (which is more in the latter case) does not compensate the excess amount of net work in configuration (e).

As expected, the losses of pump and turbine in 1PT and 2PT systems are more than the sum of pump, turbine and PX in PX systems, which makes the use of PX advantagous. However, adding the second PX to the system, despite eliminating the pump loss, makes the 2PX system less efficient. That is because the sum of pump and PX losses in the dual stage system with 1PX is less than PX losses in a 2PX system. This is in accordance with our previous findings, as discussed before.

As shown in Tables 5—7, the addition of the second hydro turbine between the modules does not increase the PD and W_{drawn} target functions. Addition of the second turbine and depressurizing the draw flow between modules only adds to work loss rather than net work. However, in all dual stage systems, net work for SE with 2HT is more than 1HT.

3.1.5. Internal performance of modules for single and dual stages systems

To better understand what takes place in membrane modules and where the improvements occur in dual stage system, changes in some parameters along the membrane are investigated and illustrated in Fig. 5. As indicated earlier, membrane length in the single stage module is the same as the total membrane length in dual stage PRO. The input values for pressures and flow rates are chosen such that maximum specific energy (SE) is obtained and the comparison is illustrated between single stage 1PX (c), dual stage with two hydro turbine - 1PX configuration (e), and dual stage with 1HT configuration (g), as shown in Table 3.

Fig. 5 shows the change of osmotic pressures in draw and feed solutions (π_D and π_F) (Fig. 5 (a) and (b)) and volumetric flow rates of draw and feed solutions (Q_D and Q_F) along the membrane coordinate (Fig. 5 (c) and (d)). It also illustrates the local water (J_{wr}) and salt transfer flow through the membrane Fig. 5 (e) and (f). All diagrams show the difference between the single stage system with PX (solid line), the dual stage system with 1PX configuration (e) (blue line for module 1, and red line for module 2) and the dual stage system with 1HT configuration (g) (blue dashed line for module 1, and black dashed line for module 2).

The osmotic pressure difference between the draw and feed solutions along with hydraulic pressure difference (π_D - π_F - ΔP) induces the driving force of fresh water passing through the membrane, see Eq. (3). At the upstream, the osmotic pressure for the draw solution (π_D) is at its highest value. As the drawn fresh water is added to the draw solution, the concentration of salt in the bulk reduces; hence, the osmotic pressure drops along the membrane. As illustrated in Fig. 5 (a), the osmotic pressure in the draw solution (π_D) for single stage and dual stage with 1HT, are almost the same. However, for dual stage system configuration (e), the π_D is less than others, specifically at the second module since the drawn fresh water added to the second module in this system is more than the others. This means that the draw solution is more diluted which results in less π_D.

On the feed side, osmotic pressure π_F increases along the membrane due to the loss of some fresh water passing through the membrane, as well as, salt being added due to reverse salt flux (notice that the flow is counter current). This increase drops J_{wr} according to Eq. (3).

As shown in Fig. 5 (c), draw solution flow rate (Q_D) increases gradually due to the addition of fresh water intake. At the end of each module, this additional flow drives the turbine to produce power (in the case of dual stage configuration (e)). However, drawn fresh water (J_{wr}) decreases along the membrane length because of smaller driving force at the downstream. Therefore, the rate of increase in Q_D drops. The optimum Q_D for dual stage 2HT configuration (e), is less than the single stage and dual stage with 1HT. This results in the major advantage of this system having higher SE value. As can be seen in Fig. 5 (e), J_{wr} is higher at the second module due to introducing fresh water at the second module and depressurizing the draw flow after the first module. The salt flow rate (J_s) in the feed solution drops along the membrane due to the dilution of the draw solution. The overall value of J_s is less in dual stage compared to single stage. There is a breakpoint at the beginning of the second module because of new fresh water entering the module between the first and second modules in Fig. 5 (f).

The trends for the dual stage 1HT system are almost similar to the single stage system. However, as can be seen in Fig. 5 (f). J_s is less than the single stage due to addition of fresh water flow to the second module. As can be seen in Fig. 5 (e) and (d), J_{wr} and the sum of Q_f in both modules are less than single stage ones which results in lower SE values. The improvement for dual stage system with 2HT can be higher depending on the membrane characteristics and membrane length in each module to confer the most advantage from the system.

4. Conclusions

In this paper, large scale dual stage PRO systems were compared to single stage PRO systems with a constant membrane area. The effect of salt passage, concentration polarization in the actual membranes, and pressure drop along the membrane were investigated. The counter-current flow system was modeled and compared. The input pressures and volumetric flow rates in draw and feed solutions were optimized such that the presented target functions were maximized.

It was found that the optimum pressures and volumetric flows depends on the target function. Also, it was observed that the specific energy in dual stage system was increased by depressurizing the draw flow where more water permeation was allowed at the second module. However, for other target functions (PD and W_{Drawn}) depressurizing by the second turbine between the modules was not effective and the maximum output was related to the dual stage system with 1HT and separated feed flows (Fig. 1 (g)).

Based on different target functions, dual stage system showed improvement compared to single stage system. These improvements varied for suggested configurations and target functions and maximum 8 % was obtained for specific energy. However, the improvements were less than the anticipated values. A thermodynamic analysis was conducted to scrutinize the losses in the module.

Addition of the second turbine, which depressurizes the draw flow entering the second module, might reduce the cost of membrane for the second module since it allows the choice of membranes operating at lower hydraulic pressures. In future research, the presented results will be compared with other commercial and laboratory membrane types with desired properties and/or changing the dimensions of modules in order to optimize the power output or fit the special cases demanded. Different sources of draw and feed solutions will also be investigated. High salinity solutions would also have higher energy densities, and processes based on these could therefore be less sensitive to the parasitic energy consumption of pumping and pretreatment.

Acknowledgments

The authors acknowledge support from the National Sciences and Engineering Research Council of Canada (NSERC), grant number RGPIN-2016-03679.

References

[1] R. Pattle, Production of electric power by mixing fresh and salt water in the hydroelectric pile, Nature 174 (4431) (1954) 660.
[2] F. La Mantia, M. Pasta, H.D. Deshazer, B.E. Logan, Y. Cui, Batteries for efficient energy extraction from a water salinity difference, Nano Lett. 11 (4) (2011) 1810–1813.
[3] S. Loeb, F. Van Hessen, J. Levi, M. Ventura, The osmotic power plant, 11th Intersociety Energy Conversion Engineering Conference, 1976, pp. 51–57.
[4] S. Loeb, Large-scale power production by pressure-retarded osmosis, using river water and sea water passing through spiral modules, Desalination 143 (2) (2002) 115–122.
[5] B.E. Logan, M. Elimelech, Membrane-based processes for sustainable power generation using water, Nature 488 (7411) (2012) 313.

[6] R.L. McGinnis, J.R. McCutcheon, M. Elimelech, A novel ammonia-carbon dioxide osmotic heat engine for power generation, J. Membr. Sci. 305 (1-2) (2007) 13–19.
[7] A. Ali, R.A. Tufa, F. Macedonio, E. Curcio, E. Drioli, Membrane technology in renewable-energy-driven desalination, Renew. Sust. Energ. Rev. 81 (2018) 1–21.
[8] A.P. Straub, S. Lin, M. Elimelech, Module-scale analysis of pressure retarded osmosis: performance limitations and implications for full-scale operation, Environ. Sci. Technol. 48 (20) (2014) 12435–12444.
[9] S.E. Skilhagen, Osmotic power? A new, renewable energy source, Desalin. Water Treat. 15 (1-3) (2010) 271–278.
[10] A.D. Wilson, F.F. Stewart, Deriving osmotic pressures of draw solutes used in osmotically driven membrane processes, J. Membr. Sci. 431 (2013) 205–211.
[11] Y.C. Kim, M. Elimelech, Potential of osmotic power generation by pressure retarded osmosis using seawater as feed solution: analysis and experiments, J. Membr. Sci. 429 (2013) 330–337.
[12] J.R. McCutcheon, R.L. McGinnis, M. Elimelech, A novel ammonia–carbon dioxide forward (direct) osmosis desalination process, Desalination 174 (1) (2005) 1–11.
[13] W. He, Y. Wang, M. Shaheed, Modelling and simulation of osmotic energy from salinity gradients: a case study from River Thames, 2013 International Conference on Renewable Energy Research and Applications (ICRERA), IEEE, 2013, pp. 907–912.
[14] K. Saito, M. Irie, S. Zaitsu, H. Sakai, H. Hayashi, A. Tanioka, Power generation with salinity gradient by pressure retarded osmosis using concentrated brine from SWRO system and treated sewage as pure water, Desalin. Water Treat. 41 (1-3) (2012) 114–121.
[15] W. He, Y. Wang, M.H. Shaheed, Energy and thermodynamic analysis of power generation using a natural salinity gradient based pressure retarded osmosis process, Desalination 350 (2014) 86–94.
[16] W. He, Y. Wang, M.H. Shaheed, Enhanced energy generation and membrane performance by two-stage pressure retarded osmosis (PRO), Desalination 359 (2015) 186–199.
[17] A. Altaee, A. Sharif, G. Zaragoza, N. Hilal, Dual stage PRO process for power generation from different feed resources, Desalination 352 (2014) 118–127.
[18] A. Altaee, N. Hilal, Design optimization of high performance dual stage pressure retarded osmosis, Desalination 355 (2015) 217–224.
[19] A.P. Straub, A. Deshmukh, M. Elimelech, Pressure-retarded osmosis for power generation from salinity gradients: is it viable? Energy Environ. Sci. 9 (1) (2016) 31–48.
[20] G. O'Toole, L. Jones, C. Coutinho, C. Hayes, M. Napoles, A. Achilli, River-to-sea pressure retarded osmosis: resource utilization in a full-scale facility, Desalination 389 (2016) 39–51.
[21] S. van der Zwan, I.W. Pothof, B. Blankert, J.I. Bara, Feasibility of osmotic power from a hydrodynamic analysis at module and plant scale, J. Membr. Sci. 389 (2012) 324–333.
[22] D. Bharadwaj, T.M. Fyles, H. Struchtrup, Multistage pressure-retarded osmosis, J. Non-Equilib. Thermodyn. 41 (4) (2016) 327–347.
[23] R.W. Baker, Membrane Technology and Applications, John Wiley & Sons, Ltd, 2004, pp. 96–103.
[24] H. Struchtrup, Thermodynamics and Energy Conversion, Springer, 2014.
[25] W.A. Phillip, J.S. Yong, M. Elimelech, Reverse draw solute permeation in forward osmosis: modeling and experiments, Environ. Sci. Technol. 44 (13) (2010) 5170–5176.
[26] N.Y. Yip, A. Tiraferri, W.A. Phillip, J.D. Schiffman, M. Elimelech, High performance thin-film composite forward osmosis membrane, Environ. Sci. Technol. 44 (10) (2010) 3812–3818.
[27] E. Nagy, A general, resistance-in-series, salt-and water flux models for forward osmosis and pressure-retarded osmosis for energy generation, J. Membr. Sci. 460 (2014) 71–81.
[28] K. Touati, F. Tadeo, Study of the reverse salt diffusion in pressure retarded osmosis: influence on concentration polarization and effect of the operating conditions, Desalination 389 (2016) 171–186.
[29] A. Altaee, A. Sharif, Pressure retarded osmosis: advancement in the process applications for power generation and desalination, Desalination 356 (2015) 31–46.
[30] Y. Wang, W. He, H. Zhu, Computational fluid dynamics (CFD) based modelling of osmotic energy generation using pressure retarded osmosis (PRO), Desalination 389 (2016) 98–107.
[31] A.A. Alanezi, A. Altaee, Enhanced performance dual stage pressure retarded osmosis, Energy Procedia 142 (2017) 4182–4197.
[32] A. Altaee, N. Hilal, Dual stage PRO power generation from brackish water brine and wastewater effluent feeds, Desalination 389 (2016) 68–77.
[33] W. He, Y. Wang, I.M. Mujtaba, M.H. Shaheed, An evaluation of membrane properties and process characteristics of a scaled-up pressure retarded osmosis (PRO) process, Desalination 378 (2016) 1–13.
[34] Y. Chen, R. Vepa, M.H. Shaheed, Enhanced and speedy energy extraction from a scaled-up pressure retarded osmosis process with a whale optimization based maximum power point tracking, Energy 153 (2018) 618–627.
[35] J. Kim, B. Kim, D.I. Kim, S. Hong, Evaluation of apparent membrane performance parameters in pressure retarded osmosis processes under varying draw pressures and with draw solutions containing organics, J. Membr. Sci. 493 (2015) 636–644.
[36] A. Altaee, G.J. Millar, G. Zaragoza, Integration and optimization of pressure retarded osmosis with reverse osmosis for power generation and high efficiency desalination, Energy 103 (2016) 110–118.
[37] A. Achilli, T.Y. Cath, A.E. Childress, Power generation with pressure retarded osmosis: an experimental and theoretical investigation, J. Membr. Sci. 343 (1-2) (2009) 42–52.
[38] S. Lee, Y.C. Kim, S.-J. Park, S.-K. Lee, H.-C. Choi, Experiment and modeling for performance of a spiral-wound pressure-retarded osmosis membrane module, Desalin. Water Treat. 57 (22) (2016) 10101–10110.
[39] Y. Tanaka, M. Yasukawa, S. Goda, H. Sakurai, M. Shibuya, T. Takahashi, M. Kishimoto, M. Higa, H. Matsuyama, Experimental and simulation studies of two types of 5-inch scale hollow fiber membrane modules for pressure-retarded osmosis, Desalination 447 (2018) 133–146.
[40] Z.L. Cheng, X. Li, Y. Feng, C.F. Wan, T.-S. Chung, Tuning water content in polymer dopes to boost the performance of outer-selective thin-film composite (TFC) hollow fiber membranes for osmotic power generation, J. Membr. Sci. 524 (2017) 97–107.
[41] H.T. Madsen, S.S. Nissen, J. Muff, E.G. Søgaard, Pressure retarded osmosis from hypersaline solutions: investigating commercial FO membranes at high pressures, Desalination 420 (2017) 183–190.
[42] C. Grace, Static mixing and heat transfer, Chem. Process. Eng. 52 (7) (1971) 57.
[43] Z. Cao, D. Wiley, A. Fane, CFD simulations of net-type turbulence promoters in a narrow channel, J. Membr. Sci. 185 (2) (2001) 157–176.
[44] M. Park, J.H. Kim, Numerical analysis of spacer impacts on forward osmosis membrane process using concentration polarization index, J. Membr. Sci. 427 (2013) 10–20.
[45] G. Schock, A. Miquel, Mass transfer and pressure loss in spiral wound modules, Desalination 64 (1987) 339–352.
[46] F. Li, W. Meindersma, A. De Haan, T. Reith, Optimization of commercial net spacers in spiral wound membrane modules, J. Membr. Sci. 208 (1) (2002) 289–302.
[47] J. Wang, D.S. Dlamini, A.K. Mishra, M.T.M. Pendergast, M.C. Wong, B.B. Mamba, V. Freger, A.R. Verliefde, E.M. Hoek, A critical review of transport through osmotic membranes, J. Membr. Sci. 454 (2014) 516–537.